JOURNAL OF THERMOPHYSICS AND HEAT TRANSFER
Vol. 21, No. 4, October–December 2007

Thermal Analysis of a Blade–Twist Actuator System

Nicholas Caldwell* and Ephraim Gutmark†
University of Cincinnati, Cincinnati, Ohio 45221
and
Robert Ruggeri‡
Boeing Phantom Works, Kent, Washington 98032

DOI: 10.2514/1.30022

Using a lumped-mass heat transfer model, predictions are made of the performance of a blade–twist actuator system that employs thermoelectric modules as both a heat source and a heat pump to effect changes in aerodynamic surfaces via shape memory alloy triggered by changes in temperature. Basic cases are presented and the ambient limitations of such a system are predicted using the model. Furthermore, means of optimizing the performance of the blade twist are investigated, as well as characterizations of how the system would perform under various startup conditions. Additional recommendations for further optimizing the system for performance under a wide variety of ambient and operating conditions are made based on simulation results.

Nomenclature

A	=	radiator area, m^2
c_p	=	specific heat, $J/kg \cdot K$
h	=	convective heat transfer coefficient, $W/m^2 \cdot K$
$\bar{h}$	=	convective heat transfer coefficient dispersed over radiator area, $\bar{h} = hA$, W/K
I	=	input current, or input current vector, A
k	=	time index
m	=	thermal zone mass, kg
N	=	number of thermoelectric modules
q	=	heat flow, W
R	=	thermoelectric module resistance, Ω
T	=	temperature of thermal zone or atmosphere, °C
T_{air}	=	ambient temperature, °C
$T_{\text{air,max}}$	=	hot-day ambient temperature limitation, °C
$T_{\text{air,min}}$	=	cold-day ambient temperature limitation, °C
T_{crit}	=	current ramp criteria temperature, °C
T_0	=	center temperature of nitinol specific heat capacity curve, °C
t	=	time, s
α	=	Peltier coefficient, V/K
β	=	temperature hysteresis constant, °C
ΔT	=	temperature difference between adjacent thermal zones, or between thermal zone and ambient air, °C
Δt	=	time step, s
κ	=	thermal conductivity dispersed over connection length, W/K
$\underline{\lambda}$	=	baseline nitinol specific heat capacity, $J/kg \cdot K$
$\bar{\lambda}$	=	latent heat capacity, $J/kg \cdot K$
σ	=	standard deviation of nitinol specific heat capacity curve, $J/kg \cdot K$

Subscripts

a	=	property corresponding to the left guard bank of thermoelectric modules
b	=	property corresponding to the shuttle bank of thermoelectric modules
c	=	property corresponding to the right guard bank of thermoelectric modules
l	=	property corresponding to the thermal zone left of thermoelectric modules
r	=	property corresponding to the thermal zone right of thermoelectric modules

I. Introduction

THE shape of an aircraft component is typically designed for optimum performance at only one specific flight condition and is subsequently unchangeable. This results in aerodynamic losses at flight conditions other than the design point. By introducing the capability of optimizing aerodynamic surfaces at other flight conditions, aircraft range and payload capabilities can be improved significantly. A recent study conducted by NASA John H. Glenn Research Center has shown a 1% savings in drag would save the U.S. wide body transport fleet approximately $140 million per year [1]. Shape optimization of turbomachinery, inlets, and chevrons could also improve engine performance characteristics [2,3] and reduce exhaust noise [4]. One manner in which aerodynamic surfaces can be reshaped is with shape memory alloys (SMAs), which respond to changes in temperature. In this manner, shape memory alloys can be trained to twist as their temperature changes. Shape memory alloys generally have a large specific work output and lightweight composite structures can be made using this material. By properly designing a composite structure, its shape can be changed as desired to optimize for different flight conditions. As such an engine inlet can be designed to be efficient at both takeoff and cruise conditions, or a wing could be twisted to fly at different altitudes without a significant performance loss. This study examines a system that can twist a wing by means of a nitinol shape memory alloy that is thermally activated when current is applied through thermoelectric modules (TEMs). A mathematical model for the heat transfer occurring within the system has been developed, and predictions are presented showing estimates of the behavior and limitations of the system. Many models were examined throughout the course of this work, beginning with a four-zone model described previously [5], and going through many transitions from a 14-zone model to a six-zone model to the final eight-zone model that will be described here. It is shown that a successful blade twist can be made under various ambient

Presented as Paper 1216 at the 45th AIAA Aerospace Sciences Meeting & Exhibit, Reno, Nevada, 8–11 January 2007; received 25 January 2007; accepted for publication 14 April 2007.

*Graduate Research Assistant, Department of Aerospace Engineering, ML0070. Student Member AIAA.
†Professor and Ohio Eminent Scholar, Department of Aerospace Engineering, ML0070. Associate Fellow AIAA.
‡Associate Technical Fellow, MS 4A-51, Seattle, WA 98124. Member AIAA.

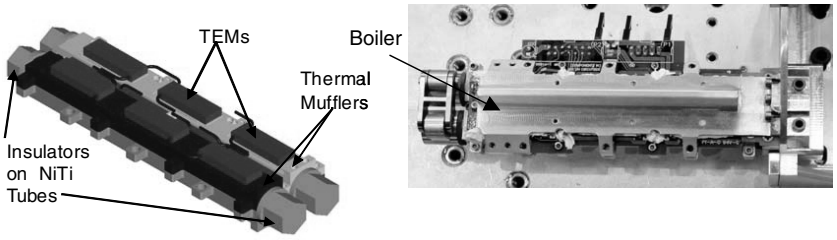

Fig. 1 Schematic and model of heat transfer actuator.

conditions, which thereby translates into a reduction in aerodynamic drag. Changes in ambient conditions can correspond to either changes in altitude or geographical location, suggesting that the blade–twist actuator system can serve a variety of purposes. For an aircraft making large changes in altitude, adjusting the wing shape based on the incoming flow will result in a performance enhancement. Likewise, an aircraft that works in diverse ambient environments would benefit from being able to modify its outer mold line to better operate under various conditions.

II. Numerical Modeling

An introduction to the numerical heat transfer model developed for this work is presented elsewhere, along with validations of its predictions [5]. After briefly summarizing the initial development of this model, a description will be provided of the additions made to the model that have rendered it more suitable to predict the performance of the blade–twist actuator system. First of all, it is necessary to describe the physical system that is being modeled. On the left of Fig. 1, a simplified diagram of the actuator system is shown, while the scale model that is being numerically modeled is shown on the right. This device fits inside an aerodynamic surface and uses the morphing of the shape memory alloy in response to heat input and extraction to contort the aerodynamic surface. Two parallel tubes composed of nitinol shape memory alloy are encased in aluminum mufflers that serve to transmit the twisting in the nitinol material to the aerodynamic surface. Furthermore, these mufflers are the sole means through which heat is conducted into the nitinol tubes themselves. Further description of the mechanical transmission of this nitinol twist to the aerodynamic surface is beyond the scope of this effort. On the left side of the physical model shown on the right of Fig. 1, the capped ends of these nitinol tubes may be discerned. The left and right mufflers are connected through a bank of four TEMs whose primary purpose is to pump heat between the two mufflers proportional to the current passing through them. In addition to this, however, the TEMs act as a source of resistive heating and a medium through which heat may be conducted between adjacent thermal zones. All of these modes of heat transfer must be taken into consideration, as will be shown later. Each muffler is in turn connected to a thermal fin through a bank of three TEMs, and the thermal fins are connected to a common boiler. The boiler is shown in the scale model in Fig. 1, but is absent from the schematic diagram. Depending on the desired nitinol tube temperature profile, heat generated by the TEMs can be pumped through the system by taking advantage of the Peltier effect and the pumping capacity of the devices. In essence the temperature profile of the system, and hence the shape of the aerodynamic surface, can be controlled by tailoring the input current profile for the desired result. The previous model consisted of four lumped-mass thermal zones connected by the three banks of TEMs just described.

Zones 1 and 2 were each defined to consist of an aluminum muffler that encased a nitinol tube, as well as half of the TEM banks on either side that were adjacent to the muffler. As such, the specific heat capacity of these zones was the mass-averaged specific heat capacity of the component parts. Because the nitinol material has a temperature dependent specific heat capacity, the overall specific heat capacity of these two zones was likewise temperature dependent. The bank of TEMs connecting these two zones is referred to as the shuttle bank. Zones 3 and 4 consisted of thermal fins, each connected to one muffler through a guard bank of TEMs. These zones exhibit a constant specific heat capacity whose mass is simply the mass of the thermal fin plus half of the mass of the adjacent bank of TEMs. In addition to the heat transfer resulting from the usage of the TEMs, convection from the thermal fins is modeled using heat transfer coefficients determined experimentally. A diagram of this model is shown in Fig. 2. Numerous cases were simulated with this model, and comparisons to experimental data have shown that temperature predictions fell within $\pm 3.5^{\circ}$C at all time steps, but for the bulk of the simulations were within fractions of a degree.

Additions to this model have since been made to better simulate the blade–twist actuator system integrated into a wing. These include a boiler section that connects the thermal fins, represented as zone 7, which in turn is connected to a radiator through which heat is dissipated, zone 8. To further simplify the model, the nitinol tubes have been separated into their own thermal zones, zones 5 and 6, removing the necessity to mass average the specific heat capacities of the muffler zones with that of the nitinol material. These changes are reflected in Fig. 3, and a brief discussion will follow concerning the development of the equations used to model the heat transfer in this system.

The heat balance in any given thermal zone in the model can be given by the following equation:

$$mc_p \frac{\partial T}{\partial t} = \sum q_i \tag{1}$$

The TEM model consists of two temperature zones, one for each side of the TEM. Each of the two zone equations contains three terms on the right, as shown below. The subscript 1 describes the thermal zone on the left of a TEM, and the subscript 2 refers to the thermal zone on the right:

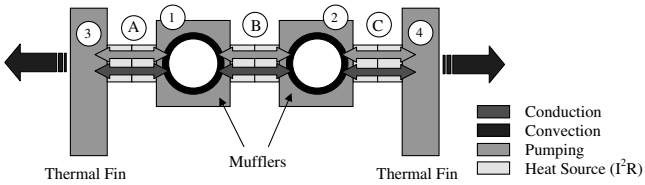

Fig. 2 Four-zone thermal model from [5].

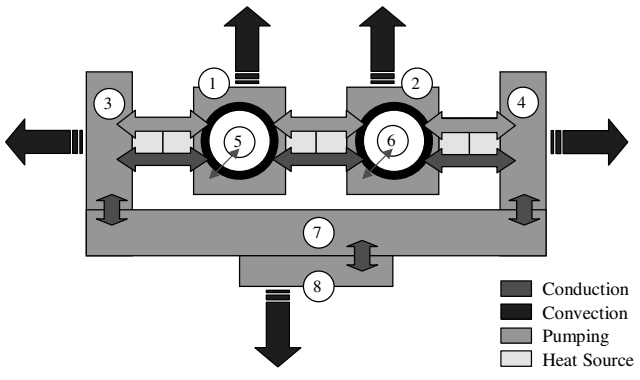

Fig. 3 Eight-zone thermal model.

$$m_l c_{pl} \frac{\partial T_l}{\partial t} = \alpha I T_l + \frac{1}{2} R I^2 - \kappa (T_l - T_r) \tag{2}$$

$$m_r c_{pr} \frac{\partial T_r}{\partial t} = -\alpha I T_r + \frac{1}{2} R I^2 + \kappa (T_l - T_r) \tag{3}$$

The temperature change experienced by the thermal zone is governed by three heat flows. The first term, involving α, is the pumped heat described by the Peltier effect. The second term represents the heat source term due to the resistance heating of the TEM, and is proportional to the square of the input current. The final term is the heat flow due to conduction that occurs when there is a temperature difference across the TEM.

In a similar fashion, we have applied Eq. (1) to each of the four zones connected to TEMs shown in Fig. 3 to develop the following four equations:

$$m_1 Cp_1 \frac{\partial T_1}{\partial t} = (N_b \alpha_b I_b + N_a \alpha_a I_a) T_1 + \frac{1}{2}(N_b R_b I_b^2 + N_a R_a I_a^2) + [N_a \kappa_a (T_3 - T_1) - N_b \kappa_b (T_1 - T_2)] - \kappa_{15}(T_1 - T_5) \tag{4}$$

$$m_2 Cp_2 \frac{\partial T_2}{\partial t} = (N_c \alpha_c I_c - N_b \alpha_b I_b) T_2 + \frac{1}{2}(N_b R_b I_b^2 + N_c R_c I_c^2) + [N_b \kappa_b (T_1 - T_2) - N_c \kappa_c (T_2 - T_4)] - \kappa_{26}(T_2 - T_6) \tag{5}$$

$$m_3 Cp_3 \frac{\partial T_3}{\partial t} = -N_a \alpha_a I_a T_3 + \frac{1}{2} N_a R_a I_a^2 - N_a \kappa_a (T_3 - T_1) - \bar{h}_3 (T_3 - T_{\text{air}}) - \bar{h}_{13}(T_1 - T_3) - \kappa_{37}(T_3 - T_7) \tag{6}$$

$$m_4 Cp_4 \frac{\partial T_4}{\partial t} = -N_c \alpha_c I_c T_4 + \frac{1}{2} N_c R_c I_c^2 + N_c \kappa_c (T_2 - T_4) - \bar{h}_4 (T_4 - T_{\text{air}}) - \bar{h}_{24}(T_2 - T_4) - \kappa_{47}(T_4 - T_7) \tag{7}$$

These equations include conduction to the thermal fins, and convection to the ambient air. It must be noted here that the nomenclature is defined such that a positive current in the left bank of TEMs (a) will result in heat being pumped from zone 3 to zone 1, a positive current in the shuttle bank of TEMs (b) will result in heat being pumped from zone 2 to zone 1, and a positive current in the right guard bank of TEMs (c) will result in heat being pumped from zone 4 to zone 2. Similarly, a negative current implies that heat is being pumped in the opposite directions as those just described. Because zones 5 and 6 are defined to be the nitinol tube itself, there is only a conduction term from the mufflers to these areas. The equations defining this heat transfer are relatively simple:

$$m_5 Cp_5 \frac{\partial T_5}{\partial t} = \kappa_{15}(T_1 - T_5) \tag{8}$$

$$m_6 Cp_6 \frac{\partial T_6}{\partial t} = \kappa_{26}(T_2 - T_6) \tag{9}$$

Furthermore, the boiler and radiator equations are simple conduction and convection equations:

$$m_7 Cp_7 \frac{\partial T_7}{\partial t} = -\kappa_{37}(T_7 - T_3) - \kappa_{47}(T_7 - T_4) - \kappa_{78}(T_7 - T_8) \tag{10}$$

$$m_8 Cp_8 \frac{\partial T_8}{\partial t} = \kappa_{78}(T_7 - T_8) + \bar{h}_8 (T_{\text{air}} - T_8) \tag{11}$$

With the large number of variables inherent in the model, there is heavy reliance upon experimental data. However this provides the additional advantage that model validation can constantly be performed. Experimental data have revealed some inherent asymmetries in the TEM performance, most notably the thermal conductivity. As such, the problem could not be reduced in half, and subsequent asymmetries are exhibited in the nitinol tube temperature predictions.

Additional features of latent heat and temperature hysteresis, noted in experimental work, have also been incorporated into the model. The temperature dependency of the nitinol heat capacity is shown in Fig. 4. To represent the latent heat effects noticed on the experimental setup, a term was added to the baseline specific heat capacity of the nitinol material at each time step:

$$\bar{\lambda}^k = \frac{|T^k - T^{k-1}|}{T^k - T^{k-1}} \frac{\lambda}{\sigma\sqrt{2\pi}} e^{\frac{-(T^k - T_0^k)^2}{2\sigma^2}} \tag{12}$$

where λ and σ, respectively, represent the baseline and standard deviation of the nitinol temperature dependency curve, and T refers to the temperature of the nitinol material. As such, the sign of the latent heat term depends on whether the nitinol is undergoing heating or cooling. The overall specific heat capacity for the nitinol material is then the sum of the baseline specific heat capacity and the latent heat term:

$$Cp(T)^k = \lambda + \bar{\lambda}^k \tag{13}$$

Hysteresis effects are contained in the mean temperature term:

$$T_0^k = 70^\circ\text{C} + \frac{|T^k - T^{k-1}|}{T^k - T^{k-1}} \beta \tag{14}$$

where β is a temperature hysteresis constant that experimental data has shown to be near 5°C. Using a time step of $\Delta t = 0.5$ s to solve the finite difference equations describing the heat transfer in the system, grid independence has been achieved. Radiator heat transfer coefficients have been taken from computational and experimental studies performed elsewhere [6]. More detailed models have been developed, including one with 14 separate thermal zones. The distinctive feature of this model was the division of each TEM bank into two thermal zones, allowing for a more advanced modeling of their behavior. After performing extensive analysis with this model, it was determined that the number of variables introduced into the system resulted in an increase in the error relative to experimental measurements over more concise models. The reason was determined to be the reliance on small details of the experiment inherent in minimizing the thermal zones. The eight-zone model has provided a good balance of representing the system while using bulk thermal properties.

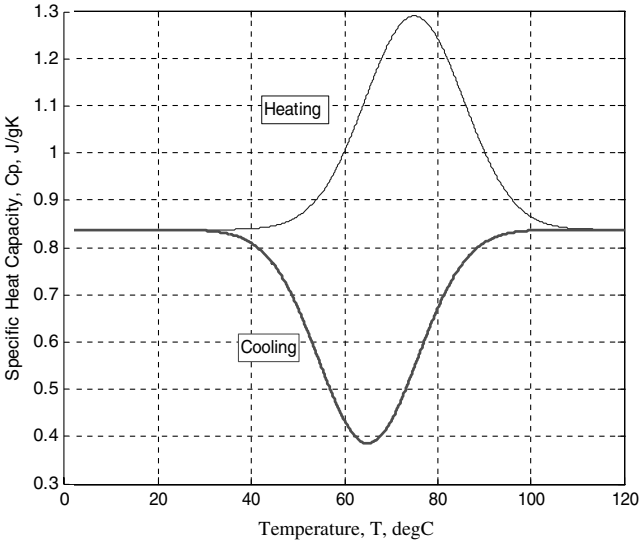

Fig. 4 Temperature dependency of nitinol effective specific heat capacity.

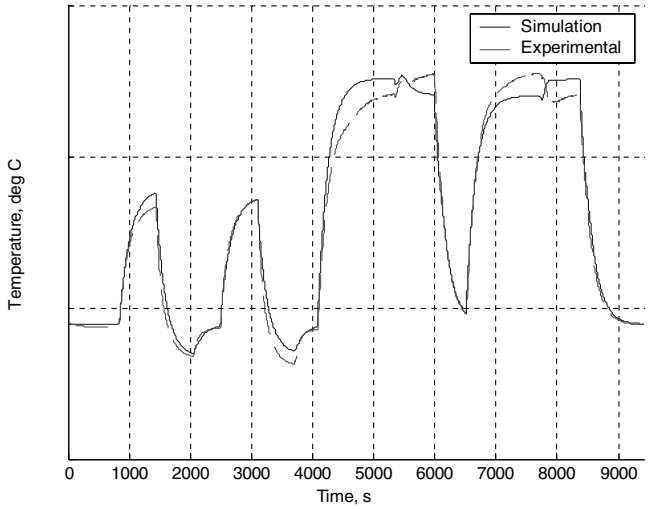

Fig. 5 Sample comparison of experimental and simulation results, $T_5 + T_6$, random input current profile.

A sample comparison between experimental data and simulation results is shown in Fig. 5. It can be seen that the majority of error occurs at extreme high temperature conditions. For this situation, the average rms error across the time of the simulation for all thermal zones was only 3.83°C, and the average maximum temperature difference for all thermal zones did not exceed 9.82°C.

III. Basic Actuator Performance

A typical warm-up cycle will show the performance of the blade–twist actuator system in terms of warm-up time and power consumption. Nitinol tube temperatures corresponding to the desired tube twist fall within separate temperature bands for each of the left and right nitinol tubes. For the left nitinol tube this corresponds to a normalized temperature range of 5.94–6.56, where the temperature is normalized by the hot-day ambient temperature limit of the actuator. For the right tube, this range becomes 1.56–2.81. Current limitations imposed on the TEM banks are ±2.5 A for the guard banks and ±3.0 A for the shuttle bank, where the sign on the current refers to the resulting direction of heat pumping through the TEM. All work presented in this paper will consider these criteria as restrictions on the system. A sample test case shows the temperature response of the nitinol tubes under particular ambient conditions with a heat transfer coefficient dispersed over the radiator area of 5.0 W/K. It can be seen in Fig. 6 that the right nitinol tube reaches its target temperature band within 424 s while the left nitinol tube reaches its higher temperature band within 1088 s. Specifically, the left and right nitinol tubes reach normalized steady-state temperatures of 6.13 and 2.68, respectively. Although the final temperatures reached are adequate, it would be optimal to reach these temperatures faster. This cycle simulated constant currents of {2.2, 1.45, 0.0} A, where the first element of the current vector describes the current in the left guard bank, the second element that of the shuttle bank, and the third element the right guard bank current. As such, the total power required for this cycle is 28.76 W, 74.05% of which is being used to pump heat between thermal zones, and the rest dissipated in the form of heat in the TEMs. The major focus of this work is to minimize the amount of time it takes for the nitinol tubes to reach their target temperature bands and expand the ambient temperature limitations of the actuator system. This being the case, investigations will be presented that allow for time-dependent current profiles, as well as variations in other system parameters which can be used to optimize performance. The major issue is dissipating heat generated inside the actuator system in an effective manner to minimize the amount of time it takes to reach the target temperatures of the nitinol tubes associated with the desired blade twist. Figure 7 shows a typical heat generation versus heat dissipation plot for a time-dependent current profile. It can be seen that there is a balance to be achieved between removing heat from the system and producing heat in the form of the TEM sources and the heat produced through the pumping action of the TEMs.

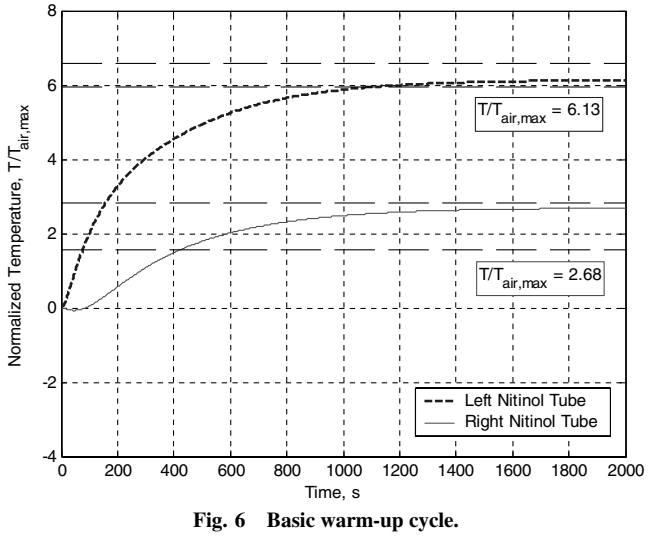

Fig. 6 Basic warm-up cycle.

IV. Ambient Temperature Limitations

To examine the ambient temperature limitations of the blade–twist actuator system, multiple simulations were run near predetermined cold and hot-day conditions. For the purposes of this work, these are defined to be $T_{\text{air,min}}$ and $T_{\text{air,max}}$, encompassing the most extreme ambient conditions that are encountered in nature. Gaining a feel for the ambient limits of this actuator will provide a sense of the operating conditions under which the actuator may function. When the ambient limits are reached in the heat transfer model, it will serve as guidance relating to the modifications that may be needed to extend these margins even further. The model also serves the additional purpose of being able to simulate ambient conditions that would otherwise be difficult in a laboratory setting.

A. Cold-Day Limitations

A simulation of the coldest day limit shows that the actuator can successfully reach the target temperature bands while still meeting the current restrictions. Taking the coldest day case of $T_{\text{air,min}}$, a constant current profile of $I = \{0.75, 2.78, 1.40\}$ A will be used with a heat transfer coefficient over the radiator area of 2.40 W/K. Although not the only valid solution for the model, this profile shows that it is feasible to achieve the target temperatures within the limits

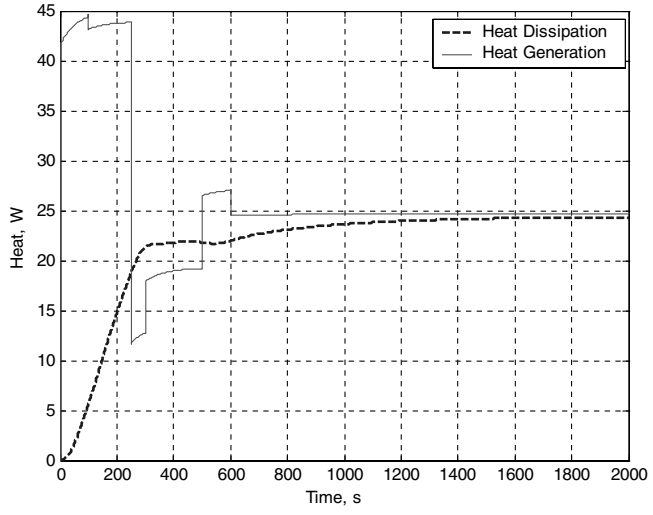

Fig. 7 Sample heat generation versus heat dissipation curve for complex current profile.

of the system. This is shown in Fig. 8, where the left and right nitinol tubes reach normalized temperatures of 5.98 and 2.73, respectively. Having a much larger temperature change to achieve than in the case presented in Sec. III, the left nitinol tube takes 1776 s to reach its temperature, and the right tube takes 651 s. Furthermore, this warm-up cycle requires a total heat generation of 42.95 W, a significant increase over the previously described case. Also of note is that a much larger percentage of this heat generation is in the form of heat dissipation in the TEMs. For this cold-day case, only 13.76% of the heat generation is due to pumping between the mufflers and fins. The amount of time that it takes to reach the target temperatures can be decreased by ramping the input currents for a short duration of time at the beginning of the cycle, but this requires more total energy. An investigation into the benefits and cost of this procedure will be discussed later.

B. Hot-Day Limitations

Numerical and experimental modeling suggests that the hot-day cases are the extreme that will result in the most difficulty in reaching target temperature bands. Simulations imply that not enough heat can be dissipated from the actuator system due to the reduction in the convection that can result from the radiator. The ΔT between the radiator and ambient temperature drops as the ambient temperature increases, and as a result the convection from the radiator is hindered. A hot-day warm-up cycle is shown in Fig. 9. It can be seen that the left nitinol tube reaches temperature in 1858 s, while the right tube takes only 306 s. Although this case takes somewhat less time to reach the target temperature bands than the cold-day case, it must be noted that the power required to complete this cycle is significantly less. Specifically, this cycle is completed using only 21.55 W and a constant current of $\{0.50, 2.10, -0.80\}$ A. Also, unlike the cold-day case, more of this power is expended in pumping heat between adjacent thermal zones than in generating heat through the TEM sources. However, it is interesting to note that any attempt to reduce the amount of time that it takes to reach the target temperatures by using more power will generally lead to overshooting the target temperatures. As a result, this ambient limit presents a problem that does not arise on the other end of the temperature spectrum. Namely, the issue of both reaching the temperature band and doing so in a timely manner arises for the case of the hot-day ambient limits, while reaching the temperature band is not an issue for the cold-day cases. On this end the only real difficulty is improving the time that it takes to arrive at the desired temperatures.

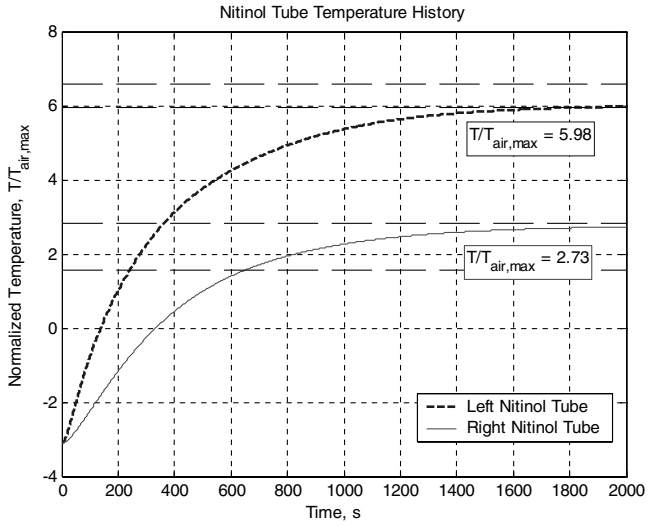

Fig. 8 Cold-day warm-up cycle.

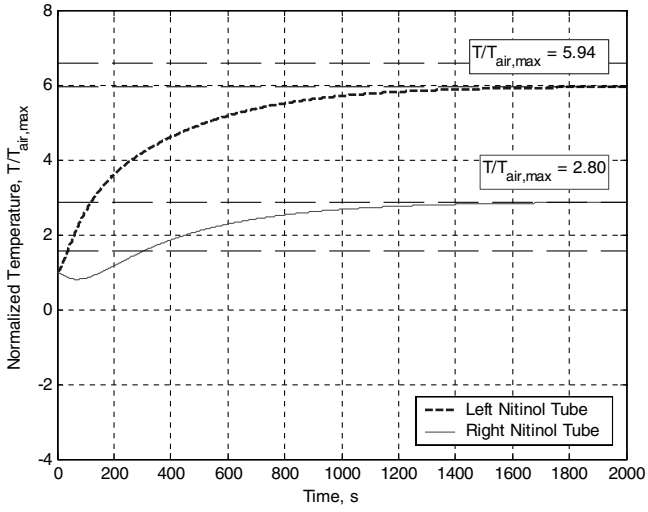

Fig. 9 Hot-day warm-up cycle.

C. Ambient Temperature Limit Extension

With the limits on the performance of the actuator system being set by the ambient temperature, a few solutions have been proposed to extend the hot-day limits. Looking at Fig. 10, an explanation for the hot-day limit becomes clear. As the ambient temperature increases, the amount of heat dissipated from the radiator decreases, as has been noted previously. However, this figure suggests that as the ambient temperature limit is approached, the amount of heat that can be dissipated from the system begins to level off. With this in mind, it can be deduced that any increase in the ambient temperature beyond this point will result in the overheating of the blade–twist actuator system as a result of the excess of heat generated in the TEM banks not being able to be dissipated.

Three solutions are proposed for increasing the hot-day limit of the actuator system. One such solution is to increase the number of TEMs in each bank, thereby increasing the heat pumping potential of one or all of the TEM banks. The other options are to vary either the size or the position of the radiator. Increasing its size will result in a larger area over which to dissipate heat, thus increasing the radiator heat transfer coefficient. Changing its position to a location with a larger heat transfer coefficient could also improve its dissipative capacity. However, simulations have shown that increasing the area or position of the radiator, that is, changing its heat transfer coefficient, only minimally affects the hot-day temperature limit of the system. This is again a result of the small temperature difference between the radiator and the ambient air during hot-day operation. These results suggest that to increase the hot-day temperature limits, the temperature of the radiator must be increased. This means heat must be transferred from the mufflers to the radiator at an increased rate. With TEMs, this implies that more energy will be transferred

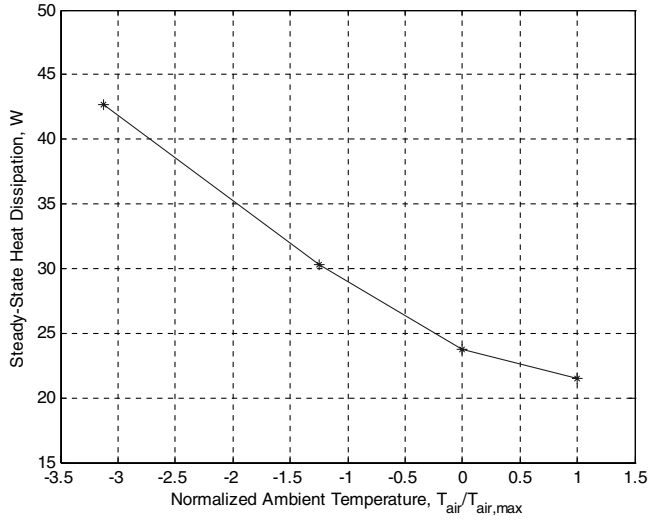

Fig. 10 Steady-state heat dissipation from radiator, $hA = 2.40$ W/K.

also. A point of diminishing returns is expected as indicated by the decreasing slope of the curve in Fig. 10. Another option which has not yet been investigated is to increase the transition temperature of the nitinol in the actuator. This would require a different alloy composition or improved heat treatments, and it would make the cold-day warm-up more difficult. In the future, the model will be used to evaluate the effects of this potential solution.

V. Decreased Time to Target Temperature Bands

A. Time-Dependent Current Profiles

The steady-state cases shown in the previous section correspond to situations in which a constant input current profile is specified for each bank of TEMs. However, in a realistic situation, it may be more suitable to reach the desired temperature bands within a shorter span of time. Depending on the application, doing so could result in reduced fuel consumption and increased range. However, this will result in an increased power requirement for the blade–twist actuator. The aerodynamic cost savings must be weighed against this power expenditure. A simple ramped current case is shown in Fig. 11 where the left nitinol tube reaches temperature 1127 s faster than in the baseline constant current case. Likewise, the right nitinol tube reaches temperature 108 s faster. This was done by ramping the current on the left guard bank of TEMs for the first 600 s of the cycle to its maximum, resulting in an increase in the total current requirement of 0.435 A for the duration of the ramp portion of the cycle. When weighed against the time savings in reaching the target temperature bands, this seems well worth the power expenditure.

Another possibility in terms of ramping currents is to allow for the maximum current restrictions to be extended for extremely low temperatures in cold-day situations. Experimental work has shown that this does not significantly degrade the TEM banks, though there is no rule defining the temperatures below which this would be acceptable. Making the assumption that the currents can be ramped up to $\{\pm 4, \pm 6, \pm 4\}$ A below a certain low criteria temperature, the reduction in the time that it takes the nitinol tubes to reach their target temperature bands can be seen in Fig. 12, measured relative to the case presented in Fig. 8. This plot assumes that when the nitinol tubes are below these criteria temperatures, the TEMs are ramped to these new maxima, but when the tube temperatures surpass the criteria, the TEMs are supplied with $\{2.5, 1.8, 1.2\}$ A. It can be seen that the tubes can reach temperature on a cold day much faster with these ramped currents. Allowing the currents to be ramped to their fullest extent below 0°C can be seen to reduce the time to target temperatures of the left and right nitinol tubes each by 488 s at the lower ambient temperature limit of the actuator. Although over 8 min worth of time is saved during which drag penalties can be reduced, the degradation of the TEMs due to this current ramping needs to be investigated to determine whether or not the benefit is worth the consequences experienced by the hardware.

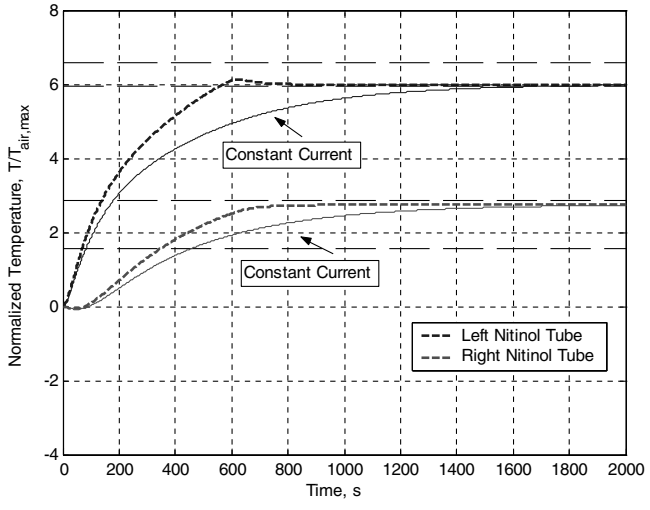

Fig. 11 Ramped current case.

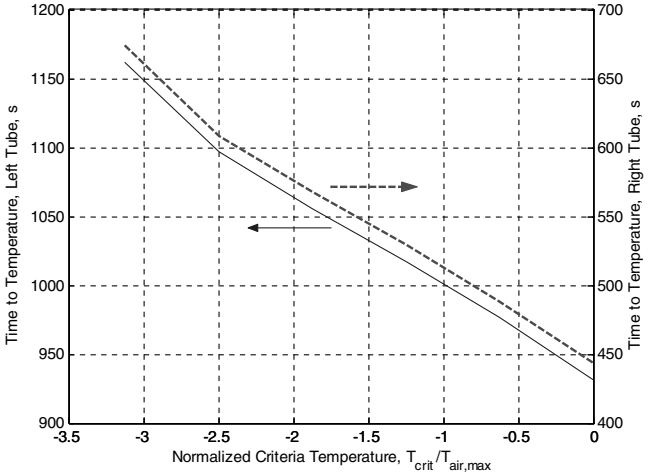

Fig. 12 Reduction in time to temperature with criteria temperature.

B. Increased Number of TEMs

A potential solution to the hardware degradation problem discussed in the previous section is to include more TEMs in actuator systems which will be exposed to cold-day scenarios on a more regular basis. An actuator with one more TEM in the left guard bank can reach its target temperatures at the cold-day ambient limit with a constant input current within the restrictions of $\{\pm 2.5, \pm 3.0, \pm 2.5\}$ A 570 s faster than the baseline actuator system. Given that there is enough physical space in the actuator, this may be a plausible means of reducing the time it takes for a system to reach its desired blade twist under cold-day conditions. On the other hand, if space is not available, ramping the currents temporarily beyond their specification may be a viable means of reducing this transition time. The additional current involved may also require a more active current control once the desired target temperature band is reached.

VI. Engine Startup Procedures

This portion of the work examines the capability of the system to operate with no heat dissipation through the radiator. For the application at hand, this refers to a situation in which the engine is not running, or serves as a limiting case as the radiator area tends to zero. For practical implementation it is extremely important to know how well the system can operate under extreme circumstances. Furthermore, there are many other applications for such a device, not all of which will have physical space for a large radiator or the ability to force convection. Under these conditions excess heat buildup inside the actuator may lead to nitinol tube temperatures that are much higher than desired. On top of this, temperature reversal cycles become difficult to perform with reduced heat dissipation capabilities. An examination of a startup procedure in which the engine is off and the blades are not rotating is described. It is simulated by using a radiator convective heat transfer coefficient of zero. The first case to be presented shows a warm-up cycle in which the blades do not turn for the first 600 s of the cycle. Then, a simulation is shown in which a temperature reversal cycle is made under the same conditions.

A. Simple Warm-Up Cycle

Figure 13 shows a warm-up cycle in which the blades do not rotate until 600 s into the cycle for an initial current of $\{1.0, 3.0, -1.0\}$ A. With no capability of dissipating heat through the radiator, the temperatures can be seen to increase at an accelerated rate. In fact, the left and right nitinol tubes reach their target temperatures in 288 and 191 s, respectively. The problem then arises that the temperatures will keep rising without any current adjustments. Hence, acquiring

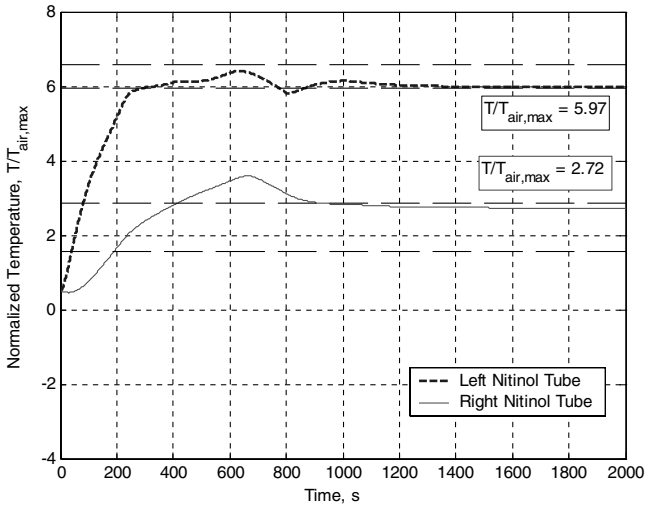

Fig. 13 Engine-off simulation—engine off until $t = 600$ s.

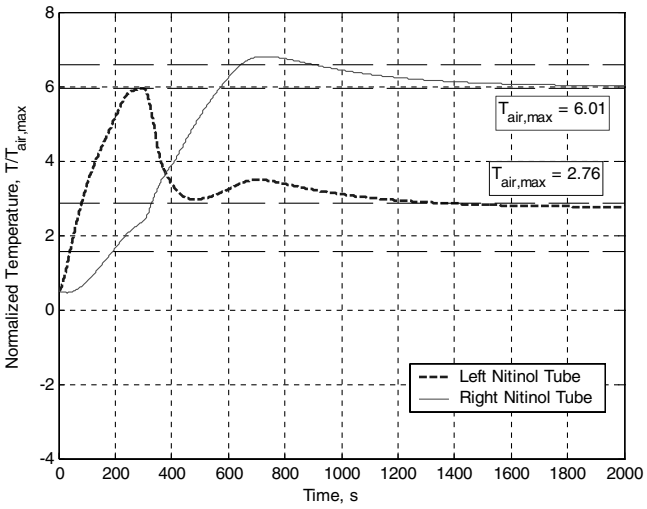

Fig. 15 Temperature reversal cycle—engine off until $t = 600$ s.

target temperatures with no dissipation capacity requires an active control of the input current. Even so, maintaining temperature inside the target bands becomes difficult without any power to remove heat from the system. This is shown by the inability to control the right nitinol tube temperature within the band in Fig. 13, and the sporadic nature of the temperature in the left tube. However, once the engine starts and the blades begin to turn, the dissipation of heat begins, and the temperature oscillations relax to a steady state within the target temperature bands. The success of this cycle is that once the blades begin to rotate, the left nitinol tube has already reached its target temperature, and the right nitinol tube can reach its target in a short time. To demonstrate the difficulty in maintaining temperature to the extent shown in Fig. 13, the current profile associated with this case is shown in Fig. 14. It can be seen that even after the blades begin to turn, 600 s into the cycle, modifications to the current are still necessary to arrive at steady-state temperatures in the target bands. However, the simulation has shown that a moderately successful blade–twist cycle can be performed before engine start.

B. Temperature Reversal Cycle

An additional maneuver that may be of use is the temperature reversal. This is generally performed by suddenly changing the direction of the input currents required for steady-state tube temperatures. However, in the case of stationary blades, the ability to perform such an action on the aerodynamic surface is hindered by the inability of the system to dissipate heat. Although there may be no practical applications of this maneuver, testing the system when the aircraft is on the ground would be extremely time consuming if the system can only slowly dissipate its heat through natural convection. In the previous section, it was shown that with the engine off for the first 600 s of the cycle, the actuator could be brought up to temperature and maintained to within a narrow range inside its target temperature band. The simulation presented here allows for the blades to be stationary for the same amount of time, but once the temperatures are reached 300 s into the cycle, the currents are reversed and the tubes are heated or cooled to their opposing temperature bands. As this requires a significant amount of heat removal from the left nitinol tube, it can be seen in Fig. 15 that immediately before the initiation of rotation, the actuator begins to overheat. This is noticeable by the increasing temperatures in the 500–600 s range. Once the blades begin turning, the removal of heat from the system results in the relaxation of the temperatures down to their steady-state values. It should be noted that due to the nature of this cycle, hitting both of the target temperature bands is extremely difficult, but both nitinol tubes fall within their goals. However, the main result to be gathered from this simulation is that a temperature reversal cycle is achievable without forcing air over the radiator to dissipate heat until well into the cycle. It is likely that low ambient temperature conditions would better support this type of cycle in that heat dissipation from the radiator could be much greater.

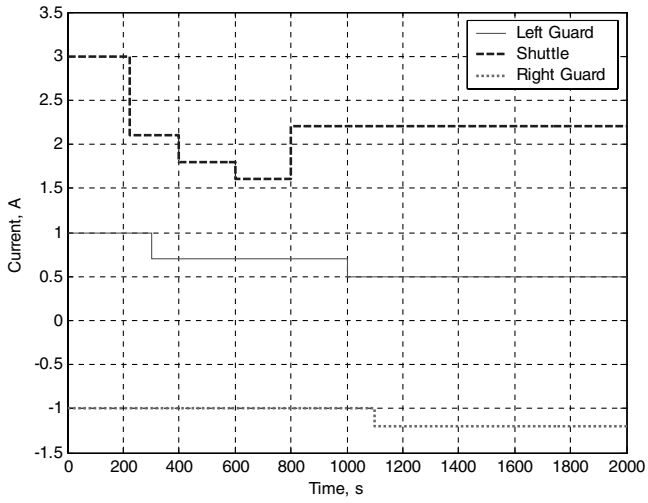

Fig. 14 Current profile associated with Fig. 13.

VII. Conclusions

An analytical model has been developed to illustrate the operational properties of a blade–twist actuator based on a nitinol shape memory alloy. The model is useful for predicting general actuator performance and for indicating trends in performance parameters. It has shown that increasing radiator size has little effect on the hot-day performance. More heat must be dissipated through the radiator either by increasing the rates of conduction to the radiator or pumping more heat to this region through other means. In this manner the temperature difference between the radiator and ambient air can be raised and more heat can be dissipated. The model shows that the actuator has little difficulty warming to operating conditions on cold days.

Another physical change that has been investigated is increasing the number of TEMs pumping heat in the actuator. The warm-up time can be reduced significantly by increasing the number of TEMs. In the future, varying the number of TEMs will also be investigated as a means of increasing operational temperature limits.

The model has also been used to illustrate the effects of different modes of operation. The model makes it clear that ramping the current within the imposed restrictions reduces the time to heat the nitinol tubes to their target temperatures. In one case presented here,

over 10 min were saved by this method. In the case of extreme cold-day conditions, temporarily ramping the current beyond its restrictions can save both time and energy. Experimental work supports this conclusion. An efficient controller has been used, and it has shown that this method can reduce power requirements by a factor of 2. The benefits of this procedure could be offset by adverse effects of high current or internal heating, but experimental efforts to evaluate negative effects have thus far shown no serious consequences to the TEMs or actuator.

In the final section of this paper, the potential for blade twist with the engine off and the blades motionless was examined. This was simulated by setting the radiator heat transfer coefficient to zero in the model, thereby suggesting that there was no air being forced over the radiator. It was shown that the nitinol tubes can reach their target temperature bands, and a warm-up cycle can be completed. Under particular conditions a temperature reversal can also be performed.

The immediate focus of future work will be to find ways to improve the performance limits of the actuator system. Allowing for a diverse range of operating conditions is vital to the effectiveness of the actuator, so that new concepts will be simulated in an effort to better understand actuator limitations and to break them down. More comparisons with the experimental model will contribute to understanding actuator operation and will determine if modeling issues or physical defects exist.

Acknowledgments

The financial support of the U.S. Naval Air Command and the Office of Naval Research has been crucial to the completion of this work. The authors acknowledge the assistance of the lab technicians who have provided experimental data against which to validate and update the heat transfer model used for the purposes of this project.

References

[1] Kota, S., Hetrick, J., and Osborn, R., "Adaptive Structures: Moving into the Mainstream," *Aerospace America*, Vol. 44, No. 9, Sept. 2006, pp. 16–18.

[2] Roglin, R. L., Kondor, S., and Hanagud, S., "Adaptive Airfoils for Helicopters," AIAA Paper 1994-1764, 21–22 April 1994.

[3] Portloch, L. E., Schetky, L. McD., and Steinetz, B. M., "Shape Memory Alloy Adaptive Control of Gas Turbine Engine Blade Tip Clearance," AIAA Paper 1996-2805, 1996.

[4] Calkins, F., Mabe, J., and Butler, G., "Boeing Variable Geometry Chevron: Morphing Aerostructure for Jet Noise Reduction," AIAA Paper 2006-2142, 2006.

[5] Caldwell, N., Gutmark, E., and Ruggeri, R., "Heat Transfer Model for Blade Twist Actuator System," *Journal of Thermophysics and Heat Transfer*, Vol. 22, No. 2, 2007, pp. 352–360.

[6] Li, G., Gutmark, E., Ruggeri, R., and Mabe, J., "Correlation of Local Heat Transfer Coefficients and Pressure on an Airfoil," AIAA Paper 2003-4202, 2003.